

Evolution of microstructure and mechanical properties of

WE43 magnesium alloy during multi-pass hot rolling

Jianlei Yang¹⁾, Yuxiang Zhai¹⁾, Taotao Kang²⁾, Minmin Fu²⁾, Songhui Wang⁴⁾, Xintong Liu¹⁾, Shijie Zhou²⁾, Wenzhuo Xie¹⁾, Wenke Wang^{1,2,3)}, and Xinhua Liu³⁾

1) School of Materials Science and Engineering, Harbin Institute of Technology, Weihai 264209, China

2) Capital Aerospace Machinery Corporation Limited, Beijing 100076, China

3) Key Laboratory for Advanced Materials Processing (MOE), Institute for Advanced Materials and Technology, University of Science and Technology Beijing, Beijing 100083, China

4) Avic Guizhou Anda Aviation Forging Co. Ltd., Anshun 561005, China

Corresponding author: Wenke Wang E-mail: 15B309020@hit.edu.cn

Abstract: The evolution of microstructure and mechanical properties of WE43 magnesium alloy during multi-pass hot rolling was investigated. Results revealed that multi-pass hot rolling promoted the formation of small second phases and this was conducive to the multiple dynamic recrystallization, consequently improving the microstructure homogeneity and refining the average grain size to 8.83 μm from 34.3 μm of the initial material. Meanwhile, the rolling deformation rotated abundant grain c-axes toward the normal direction and one strong fiber texture developed. Owing to the fine-grained strengthening, second phase strengthening, and texture modification, the yield strength along the rolling direction (RD) was improved to 324 MPa in the Pass 3 sheet from 164 MPa in the initial material. In addition, the deformation mechanism distribution maps indicated that the yield strength anisotropy between the RD and the transverse direction (TD) was attributed to the effects of the texture component on the dominant mechanisms. During the tensile test, the dominant deformation mechanism was the prismatic slip affected by RD strong basal texture, while was less proportion of prismatic slip under the influence of TD weak basal texture. Compared to the basal slip, the higher critical resolved

shear stress of prismatic slip made the increase in yield strength along the RD higher about 51 MPa than that along the TD (RD: 160 MPa, TD: 109 MPa).

Key words: WE43 magnesium alloy; multi-pass hot rolling; grain size; texture; deformation mechanism

1. Introduction

Magnesium alloys have been widely used in aerospace, automotive industry, electronic devices, and biomedical fields due to their low density, high specific strength, and excellent electromagnetic shielding performance[1–4]. However, their disadvantages of low absolute strength and poor formability seriously limit their widespread commercial usability[5–6]. In response to these limitations, rare earth alloying could significantly improve the strength and formability of magnesium alloys based on solution strengthening[7], precipitation strengthening[8] and so on.

Based on the principle of rare earth alloying, WE43 magnesium alloy has excellent biocompatibility and is widely used in the field of biomedical application[9]. With such magnesium alloy, Liu et al. successfully prepared the biodegradable scaffold microtubules with 3.00 mm outer diameter and 180 μm thickness which had been used in biomedical applications[10]. Nevertheless, the low strength and poor formability of the WE43 alloy are still the key factors limiting its widespread application[9].

To further improve the strength and formability of WE43 magnesium alloy, plastic processing technology is an effective way owing to its positive role of grain refinement and texture modification. For example, Martynenko et al. refined the grain size to 0.7-1 μm in WE43 alloys by means of the equal channel angular processing (ECAP) producing the noticeable fine-grained strengthening and subsequently contributing the excellent mechanical properties with the yield strength of 260 MPa and

ductility of 13.2%[11]. Similarly, Amani et al. used the cyclic expansion extrusion (CEE) to not only refine the grain size but also develop the bimodal texture component, improving the yield stress and the elongation to 330 MPa and 17%, respectively[12]. By comparison, Liu et al. employed the single-pass rolling to obtain the WE43 alloy sheets whose yield strength was solely 269 MPa and the fracture elongation was only 0.9%[13]. Obviously, the mechanical property of the rolled WE43 magnesium alloy is not up to that of the as-extruded. The reason might be attributed to the poor plastic processing ability of the WE43 magnesium alloy, which made it crack very easily and only subject to the small deformation rolling. This severely influenced the effect of plastic deformation on the grain refinement, texture modification and precipitation tailor, weakening their improvement role in the strength and formability. With this regard, our previous works demonstrated that the multi-pass hot rolling could fully refine the grain size and modify the texture components in ZK60 magnesium alloy sheet, which improved the yield strength to 247 MPa and the fracture elongation to 17.6%[14]. However, for the WE43 magnesium alloys, the microstructure evolution as well as its role in the mechanical properties was still unclear during the entire multi-pass hot rolling, and this was considered to be the fundamental issue if we want to further improve the mechanical properties of the WE43 magnesium alloy by rolling deformation.

Therefore, this work focuses on the microstructure evolution of WE43 magnesium alloys during the multi-pass hot rolling. Meanwhile, the effect of microstructure evolution on the mechanical properties was analyzed with the help of deformation mechanism distribution maps.

2. Experimental

The initial materials used in this experiment were as-extruded WE43 alloy sheets with dimensions of 87 mm in width and 15 mm in thickness. The nominal composition of the initial material was Mg-

4.3wt%Y-2.4wt%Nd-0.5wt%Gd-0.5wt%Zr. Fig. 1a showed the schematic illustration of multi-pass hot rolling process. Before the rolling process, the sheets were preheated to 623K for 30 minutes and the rollers were heated to 493K. Then the sheets were rolled from 15 to 3 mm in the thickness by 3 passes. The sheets were annealed for five minutes between passes. The deformation of the rolling pass was 40%, and the rolling speed was 5 m/min. The rolling process parameters were shown in Table 1. During the rolling process, a contact temperature measuring device was used for temperature measurement, and the rolled plate was water-cooled. There were no obvious cracks on the surface and edges of the final rolled sheets. The resulting sheets after multi-pass hot rolling were denoted as Pass 1, Pass 2 and Pass 3 sheet, respectively.

As shown in Figs. 1b and 1c, the tension samples were extracted from the core region of the resulting plates along the rolling direction (RD) and the transverse direction (TD), and they exhibited a dog-bone shape whose gauges were 15 mm in length, 4 mm in width and 2 mm in thickness. Before measuring the mechanical properties, the surface and sides of the samples were polished to ensure that the samples were smooth, free from coarse scratches and obvious defects. Uniaxial tension tests along the RD and TD were carried out on MTS E45.105 electronic universal testing machine with an initial strain rate of $6.67 \times 10^{-4} \text{s}^{-1}$ under the room temperature.

Table 1. Multi-pass hot rolling parameters of WE43 magnesium alloy

Pass No.	Preheating temperature/K	Thickness variation/mm	Thickness reduction/%	Temperature after rolling/K
1	623	15→9.2	39	543
2	623	9.2→5.3	42	525
3	623	5.3→3.0	43	510

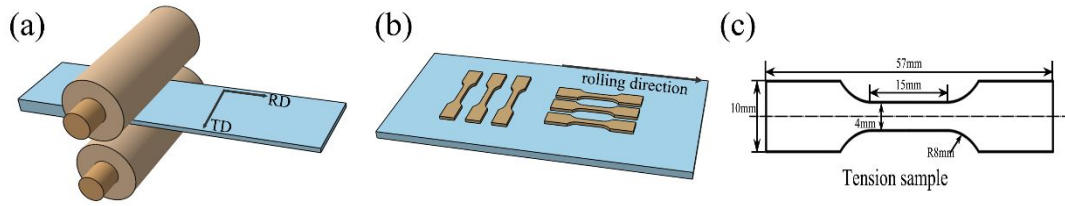


Fig. 1. Multi-pass hot rolling (a); Sampling strategy for tension test (b); Size of tension samples (c).

The microstructure characteristics were performed by scanning electron microscope (SEM) and electron backscattered diffraction (EBSD). The SEM samples were prepared by polishing and mechanical polishing, and then corroded in the 8% HNO_3 solution for 10 seconds. The corroded samples were cleaned by ultrasonic vibration in the ethanol solution. The EBSD samples were prepared by mechanical polishing, followed by electrolytic polishing. The electrolytic polishing solution was a mixture of H_3PO_4 and $\text{C}_2\text{H}_5\text{OH}$ with the volume ratio of 3:5. First, the EBSD samples were subjected to the solution of 0.5A for 2 minutes, and then operated at 0.25A for 5 minutes. After electrolytic polishing, it was sequentially cleaned by ultrasonic vibration in CH_3OH , the mixture solution of CH_3OH and $\text{C}_3\text{H}_6\text{O}$, and $\text{C}_2\text{H}_5\text{OH}$. When conducting EBSD testing, the working voltage of 20kV and the working distance of 15 mm with the sample tilt angle of 70° were selected. To ensure the accuracy of the experimental results, three experiments were conducted under each condition.

3. Results and discussion

3.1. Microstructure characteristics

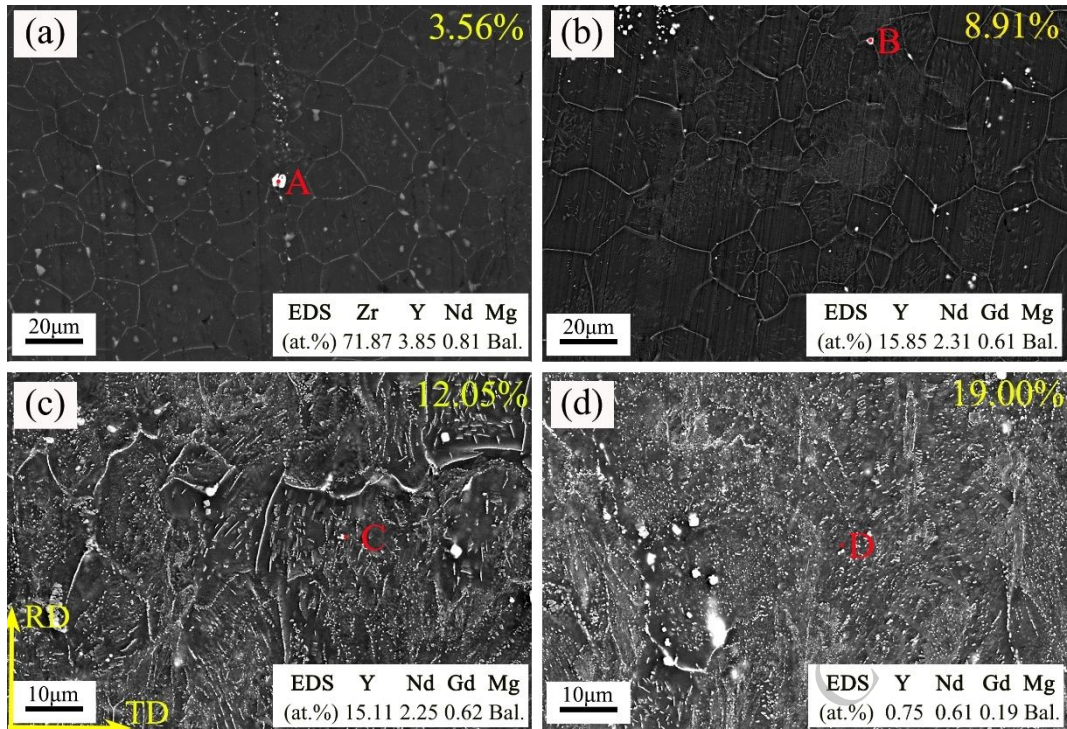


Fig. 2. SEM images and the corresponding EDS of WE43 magnesium alloy during multi-pass hot rolling: (a) Initial; (b) Pass 1; (c) Pass 2; (d) Pass 3.

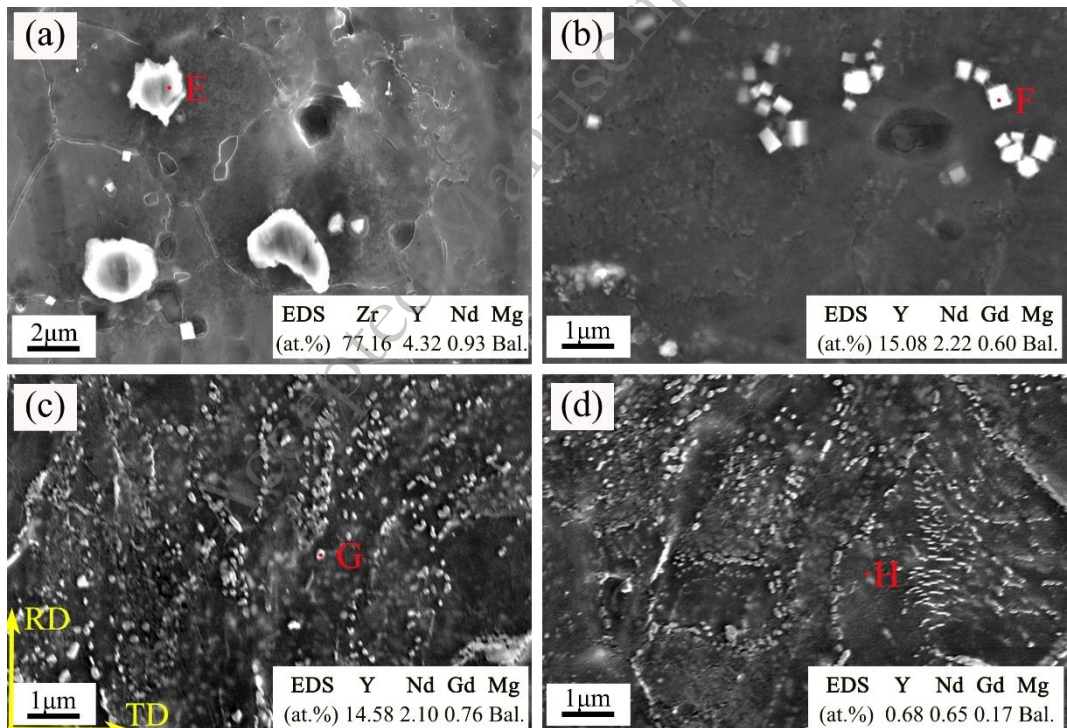


Fig. 3. High-magnification SEM images and the corresponding EDS of WE43 magnesium alloy during multi-pass hot rolling: (a) Initial; (b) Pass 1; (c) Pass 2; (d) Pass 3.

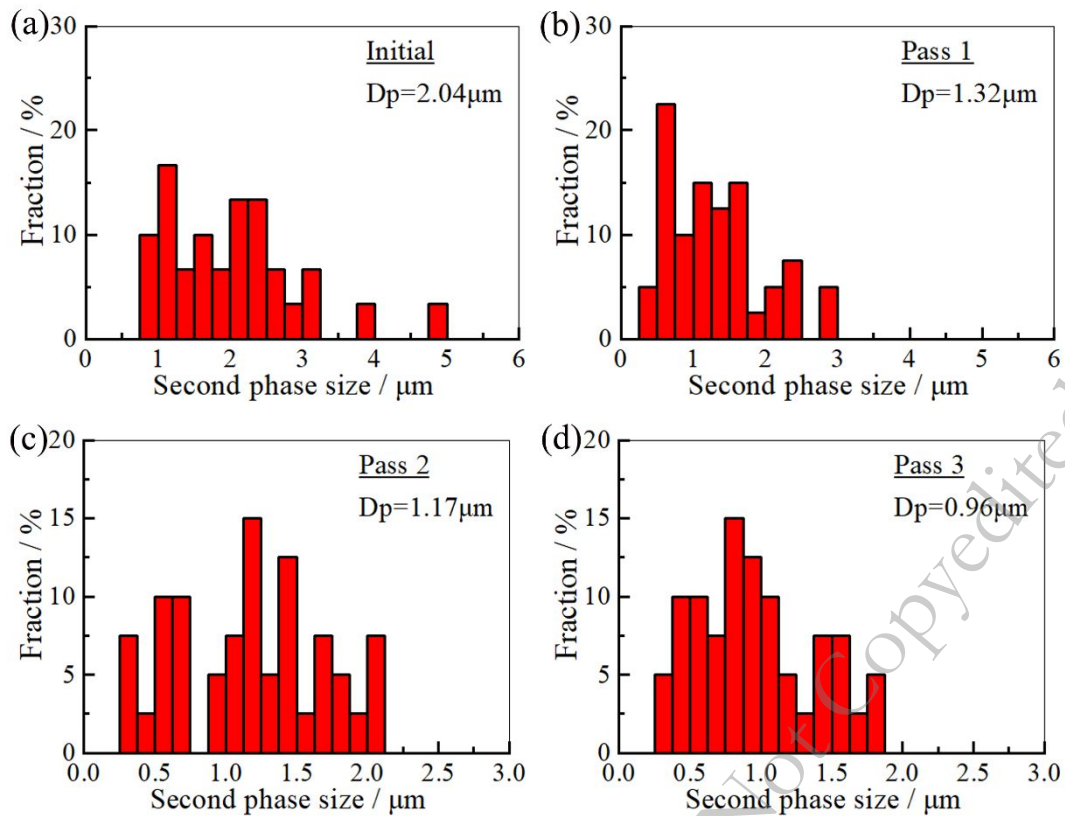


Fig. 4. Second phase size distributions of WE43 magnesium alloy sheets during multi-pass hot rolling:

(a) Initial; (b) Pass 1; (c) Pass 2; (d) Pass 3.

Figs. 2 and 3 showed the SEM observation results and the corresponding EDS of WE43 magnesium alloy during multi-pass hot rolling. Fig. 4 showed the second phase size distributions. Clearly, there only existed a small number of second phase particles in the initial material and the volume fraction was about 3.56% (Fig. 2a). Among them, most of these second phases were distributed in a network pattern along the grain boundaries with the sizes of about 2~6 μm , and a small amount of blocky phases were scattered inside the grains with the sizes of about 1~3 μm . In addition, the EDS results showed that a small amount of the second phases existed in the initial material, which were enriched in Zr. The average size of the second phase was about 2.04 μm . Compared to the initial material, there were some bright second phases in the matrix and smaller second phase particles appeared inside the grain after the first pass. Meanwhile, the volume fraction of the second phase

increased to 8.91% and the average second phase size was reduced to 1.32 μm . Dobkowska et al. once presented the similar phenomenon where the bright second phases with irregular shapes were enriched in Nd, and the phases that have sharp edges were composed of Y and Nd[15]. As the rolling continued, the number of precipitated phase particles continued to increase and their distribution became more uniform. Most of them were distributed within the matrix, with a small portion still located at grain boundaries. Moreover, the size of the newly precipitated second phases was much smaller, about 0.5~2 μm . Finally, the volume fraction increased to 19.00% and the average second phase size was reduced to 0.96 μm after the third pass. Furthermore, these second phases were generally considered as the Mg_{24}Y_5 according to many literatures[16–18], corresponding to the above EDS results in our work.

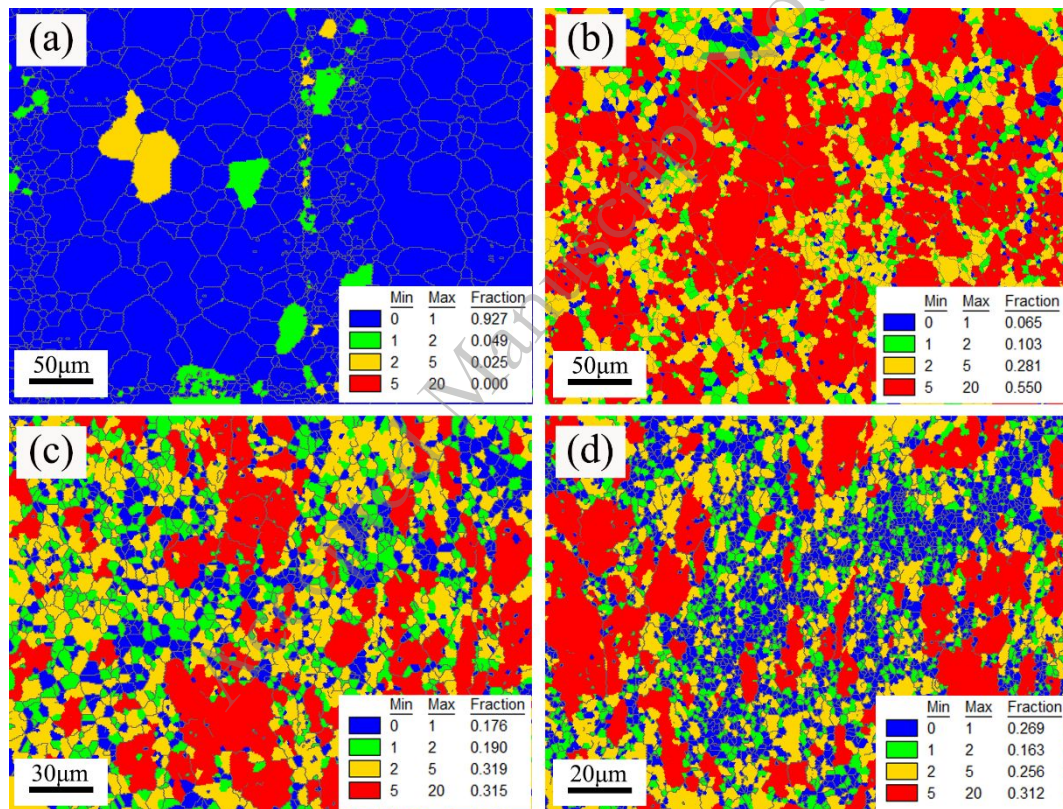


Fig. 5. Grain orientation spread (GOS) maps of WE43 magnesium alloy sheets during multi-pass hot rolling: (a) Initial; (b) Pass 1; (c) Pass 2; (d) Pass 3.

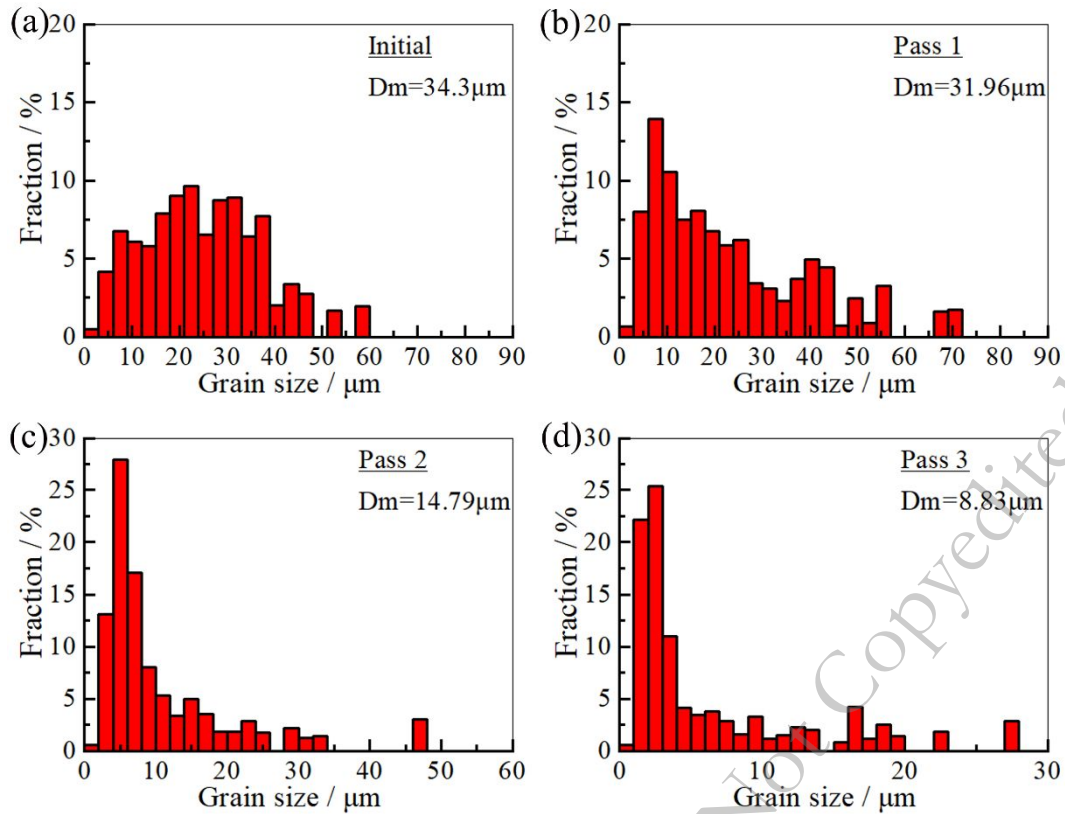


Fig. 6. Grain size distributions of WE43 magnesium alloy sheets during multi-pass hot rolling: (a) Initial; (b) Pass 1; (c) Pass 2; (d) Pass 3.

Fig. 5 showed the grain orientation spread (GOS) of WE43 magnesium alloy during multi-pass hot rolling. In this experiment, grains with GOS values smaller than 2° were defined as recrystallized grains (blue and green grains), while grains with GOS values greater than 2° were defined as grains that had not undergone complete recrystallization (yellow and red grains)[19–20]. Fig. 6 showed the corresponding grain size distribution. Obviously, the initial material consisted of coarse and fine grains, and the coarse grains were surrounded by the small equiaxed grains (Fig. 5a). Such microstructure characteristics were consistent with the wide range of grain size distribution from 1.5 μm to 60 μm (Fig. 6a). This also shows that the distribution of grain size was uneven, and the average grain size of the initial extruded alloy was 34.3 μm .

After the first pass, the sheet almost possessed one deformed microstructure whose recrystallized

grains percentage was only 16%. This was very likely to be the stored energy was not enough to activate the complete recrystallization due to the small amount of deformation and high temperature. As a result, its average grain size was marginally refined to 31.96 μm from 34.3 μm in the initial material. In addition, the second phase was an important factor by means of restricting grain boundary mobility and increasing the DRX nucleation rate[21–22]. However, the content of the second phase was relatively small after the first pass. Therefore, the effect of the second phase on the dynamic recrystallization and the subsequent grain refinement might be small during the first rolling pass.

Fig. 5c presented the microstructure morphology of the Pass 2 sheet in which percentage of the deformed grains (yellow and red grain) decreased to 63% while that of the DRXed grains increased to 37%. As the rolling progressed to the second pass, the deformation stored energy continued to increase, and this was prone to produce more recrystallization nucleation sites in multiple regions of the microstructure. These nucleation sites developed more at the grain boundaries of coarser grains, and therefore the small equiaxed grains appeared around coarser grains. In addition, the second phase increased obviously during the second rolling pass (Fig. 5c), producing the stronger pinning effect to the grain boundaries and inhibiting the growth of the DRXed grains. As a result, under the combined effects of accumulated deformation and abundant second phases, the average grain size was significantly refined to 14.79 μm in the Pass 2 sheet.

As the rolling continued, the cumulative deformation increased. Dynamic recrystallization continued to occur, and the proportion of recrystallized grains further increased, reaching 43%. The percentage of fine grains had significantly increased after the third pass. In addition, the number of the second phase particles increased to the maximum after the third pass. Such small second phase particles led to the boundaries of the DRXed grain migrating hardly and promoted the development of

a finer microstructure[23]. Therefore, the uniformity of the microstructure had also been significantly improved compared to the first and second passes. The average grain size was eventually refined to 8.83 μm .

3.2. Texture characteristics

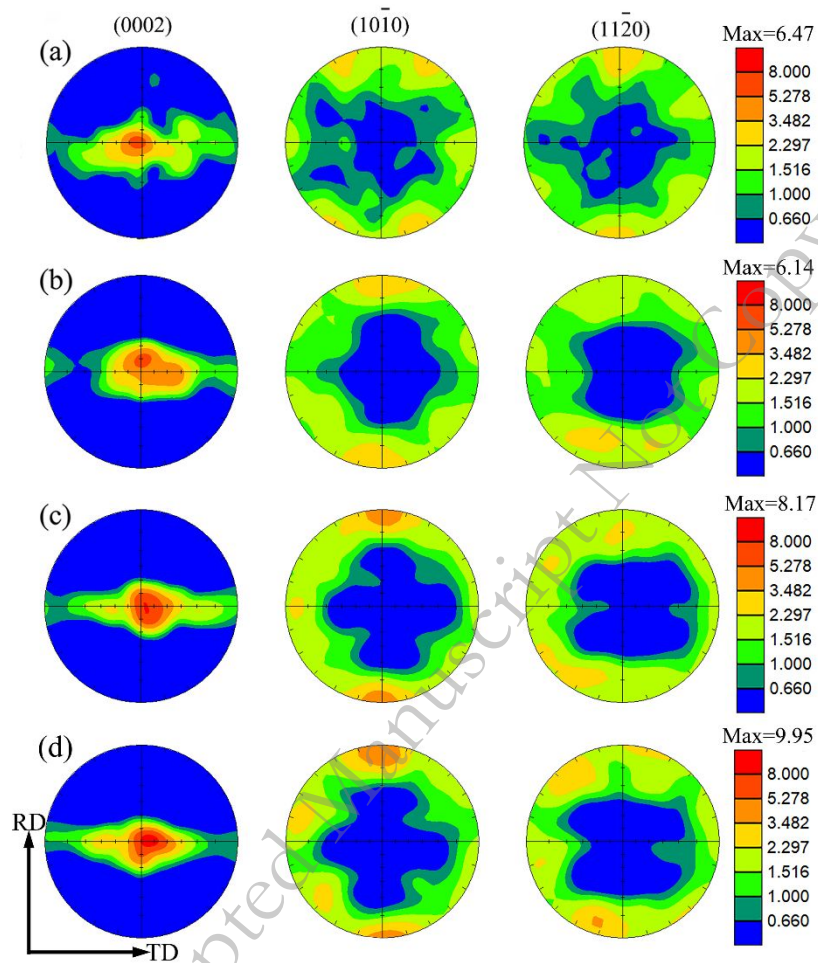


Fig. 7. (0002), (10-10) and (11-20) pole figures of WE43 magnesium alloy sheets during multi-pass hot rolling: (a) Initial; (b) Pass 1; (c) Pass 2; (d) Pass 3.

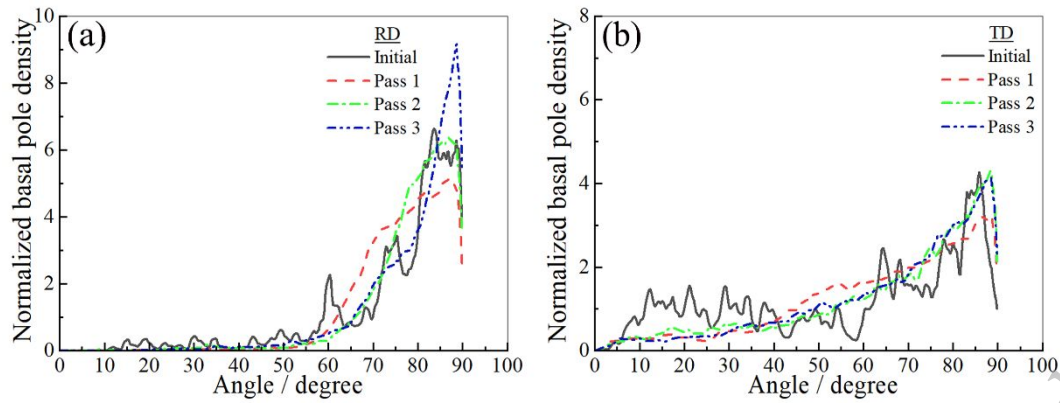


Fig. 8. (0002) pole density distributions of WE43 magnesium alloy sheets during multi-pass hot rolling: (a) RD; (b) TD.

Fig. 7 showed the (0002), (10-10), and (11-20) pole figures of the WE43 magnesium alloy during multi-pass hot rolling, revealing the texture variations of WE43 magnesium alloy during the rolling process. As shown in the (0002) pole figure (Fig. 7a), the initial material possessed one extrusion fiber texture with the texture intensity of about 6.47, in which most of the grain c-axes were spread along the TD. Meanwhile, the spread angle of the basal poles along the RD in the (0002) pole figure concentrated at -50° to 45° , clearly showing the preferred orientation. In addition, the initial material presented a six-fold symmetry texture[24–25] in the (10-10) pole figure.

After the first pass, the c-axis of the grains rotated in the ND direction. As a result, the sheet exhibited a transitional texture pattern between the extruded fiber texture and the rolled basal texture with a maximum intensity of 6.14. It was noteworthy that such a texture state was an egg-shaped asymmetric distribution[26] of the basal poles from the ND instead of the symmetric distribution on the RD-TD plane, in which more c-axes were spread along the TD than along the RD. Additionally, one strengthened $\langle 10-10 \rangle // \text{RD}$ texture component began to develop in the (10-10) pole figure, meaning that many crystal orientation of $\langle 10-10 \rangle$ were parallel to the RD.

As the rolling continued, more grain c-axes rotated to the ND and a strengthening zone was

developed in the central region of the (0002) pole figure. Meanwhile, the maximum texture intensity increased to 9.95 from 6.14 (Pass 1) and the spread angle of the basal pole along the RD slightly narrowed to -40° to 30° from -50° to 45° (initial material). The reason for these phenomena could be attributed to the synergistic effect from the activation of the deformation mechanism and the stress/strain state in the rolling process. Basal slip is the main slip system in magnesium alloys owing to its lowest CRSS. Under the comprehensive action of rolling tension and normal pressure, the (0002) basal plane gradually turned to the RD-TD plane, so that the (0002) basal plane diffuse dispersion in the TD gradually decreased. Additionally, Wang and Huang reported that the (10-10) pole of the rolled HCP metals and alloys, possessing c/a ratio less than 1.633 such as Ti, tended to align with the rolling direction due to the activation of prismatic slip[27]. Therefore, more and more $\langle 10-10 \rangle$ //RD grains appeared during the multi-pass hot rolling.

In order to clearly describe the anisotropy of texture between RD and TD and further prove the grain rotation during multi-pass hot rolling, the corresponding (0002) random numbers along RD and TD were obtained from the (0002) pole diagram in Fig. 7, and the data was normalized and organized. The random numbers were divided by $\int_0^{\pi} I \cos \theta d\theta$ (I is the intensity, θ is the angle away from RD or TD) to obtain normalized pole density distribution[26,28], as shown in Fig. 8. The angle in the figure referred to the angle between the c-axis of the grain and RD or TD, with 1.5 being the critical extreme density value for preferred orientation[28]. Obviously, there was a distinct difference in (0002) basal pole density distributions between the RD and the TD. The preferred orientation clearly strengthened in the angle range of $59-90^{\circ}$ along the RD with the maximum pole density of 6.65 (Fig. 8a) while a broad spread of basal pole with the maximum pole density of 4.27 along the TD (Fig. 8b). Importantly, along the RD, the distributions of (0002) basal pole tended to concentrate, and their

preferred orientation angle regions gradually shrank, namely 64-90° for the Pass 1 sheet, and 69-90° for the Pass 2 and Pass 3 sheets. The maximum pole density continued to increase, reaching 5.1 (Pass 1), 6.4 (Pass 2), and 9.3 (Pass 3), respectively. These results indicated that the basal texture orientation gradually concentrated and deviated towards the ND direction. Similarly, along the TD, the regions of preferred orientation angle decreased, which was 52-90° for the Pass 1 sheet and 62-90° for the Pass 2 and Pass 3 sheet, respectively. The maximum pole density increased from 3.2 (Pass 1) to 4.3 (Pass 2 and Pass 3). However, the adjustment of the diffuse texture of the TD by multi-pass hot rolling was weaker than that of the RD.

3.3. Mechanical properties

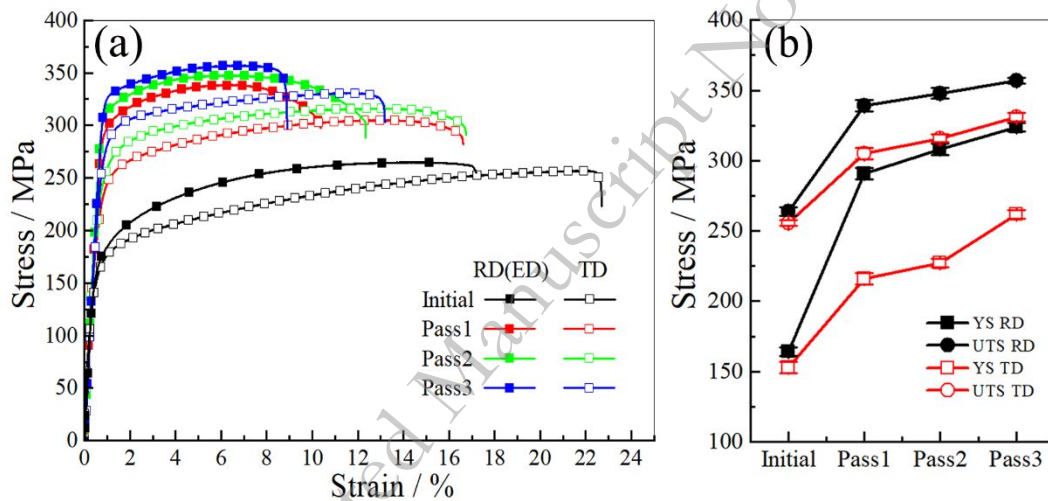


Fig. 9. Stress–strain curves of WE43 magnesium alloy sheets during multi-pass hot rolling (a); Yield strength (YS) and ultimate tensile strength (UTS) variations for different states (b).

Table 2. Mechanical properties of WE43 magnesium alloy sheets during multi-pass hot rolling

Sample	YS/MPa		UTS/MPa		UE/%		FE/%	
	RD	TD	RD	TD	RD	TD	RD	TD
Initial	164±3	153±4	264±3	256±2	14.5±0.4	21.8±0.4	17.2±0.4	22.7±0.4
Pass 1	291±4	216±4	339±4	305±4	6.1±0.3	13.2±0.3	10.4±0.3	16.6±0.3
Pass 2	308±4	227±3	348±4	316±3	6.6±0.3	12.9±0.4	12.3±0.3	16.8±0.4

Pass 3	324±3	262±3	357±2	331±3	6.6±0.3	11.4±0.2	8.9±0.3	13.2±0.2
--------	-------	-------	-------	-------	---------	----------	---------	----------

The mechanical properties were clearly illustrated in the room-temperature stress–strain curves along the RD and TD, as shown in Fig. 9a. The corresponding data for the yield strength (YS, MPa), ultimate tensile strength (UTS, MPa), uniform elongation (UE, %) and fracture elongation (FE, %) were summarized in Table 2. Clearly, all the stress-strain curves exhibited a power-curve shape[26,29] in which the material displayed stress hardening behavior after the yield stress and changed into stress softening behavior after the ultimate tension stress. Knezevic et al. reported that this shape was induced by slip-dominated deformation at the initial stage of tension deformation[30]. As mentioned above, RD possessed a stronger basal texture than TD for the initial material, and so the basal slip or (10-12) tension twin activated easily during the tension test along TD, which would result in lower stress (YS: 153 MPa and UTS: 256 MPa) but higher elongations (UE: 21.8% and FE: 22.7%) along the TD compared to mechanical properties (YS: 164 MPa, UTS: 264 MPa, UE: 14.5% and FE: 17.2%) along the RD[31]. Fig. 9b showed the YS and UTS variations during multi-pass hot rolling. According to Fig. 9b and Table 2, as rolling proceeded, the YS and UTS along the RD significantly increased to 324 MPa and 357 MPa and those along the TD increased to 324 MPa and 357 MPa similarly. Instead, the UE and FE along the RD decreased to 6.6% and 8.9% and that along the TD decreased to 11.4% and 13.2%, respectively.

Generally speaking the mechanical properties were mainly dependent on their own microstructure states[32]. Prior results suggested that there existed three kinds of microstructure variation including second phase particle, grain size and texture state. Multi-pass hot rolling produced abundant relatively small second phase particles, and their total fraction increased significantly especially after the second pass. This meant that precipitation strengthening could be an important factor to improve the strength

of the WE43 magnesium alloy. Meanwhile, the grain size was significantly refined to 8.83 μm from 34.3 μm during multi-pass hot rolling, so the YS was also significantly improved according to the Hall–Petch relationship. In addition, previous results showed that the maximum texture intensity gradually increased as the rolling progressed, which could contribute to increasing the strength of WE43 magnesium alloy based on texture strengthening. To sum up, grain refinement, texture modification and precipitation tailor could improve the YS and UTS.

However, this improvement was clearly not synchronous between the RD and the TD. Revealing this question needed to analyze the microstructure anisotropy between the RD and the TD. Obviously, previous results showed that there existed small differences in the grain size and second phase size between the RD and the TD, and therefore they might not be the major factors causing the above large mechanical properties anisotropies. Therefore, the main reason was considered to be the texture state.

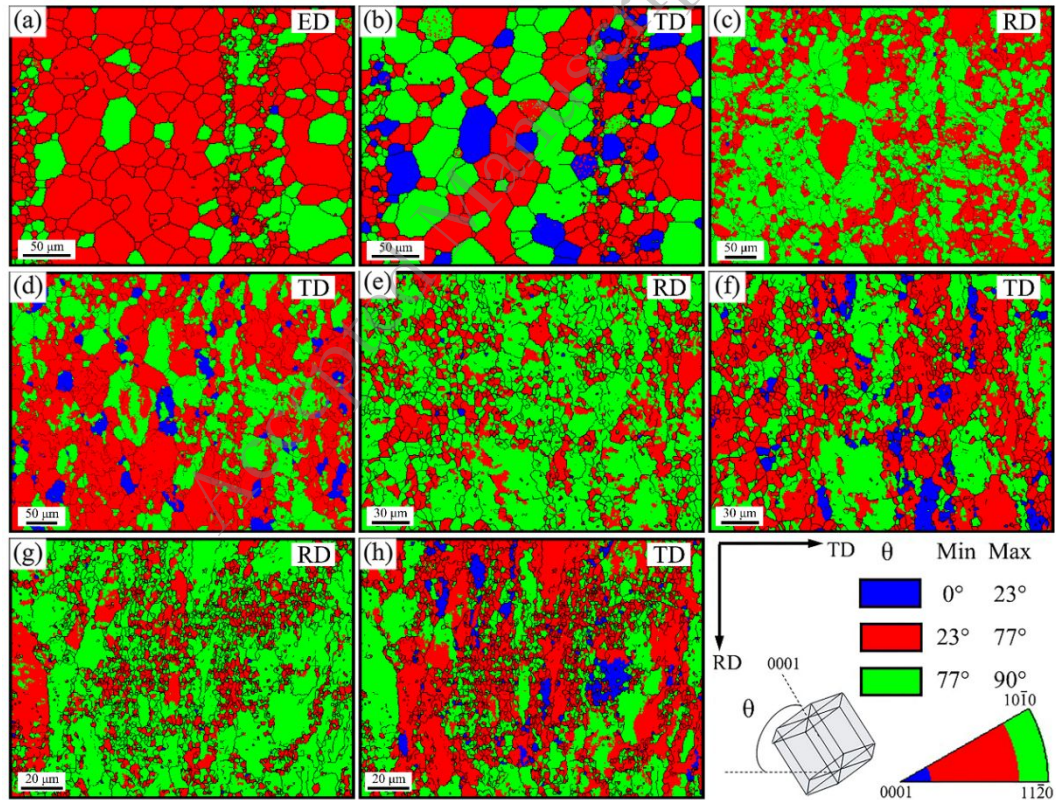


Fig. 10. Orientation distributions of WE43 alloys using grain orientation maps: (a, b) Initial; (c, d) Pass

1; (e, f) Pass 2; (g, h) Pass 3 (In grain orientation map, the grains with the $\langle 0001 \rangle$ away from the tension direction in the angle ranges of $0^\circ\text{--}23^\circ$, $23^\circ\text{--}77^\circ$ and $77^\circ\text{--}90^\circ$ were depicted by blue color, red color and green color, respectively).

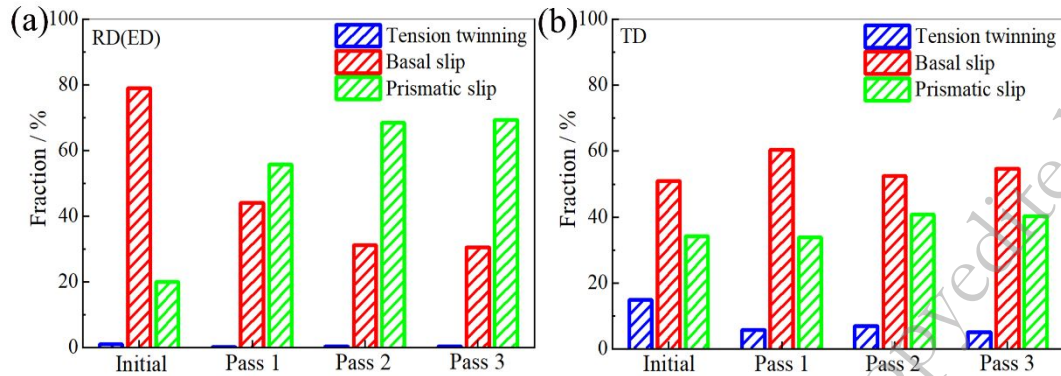


Fig. 11. Prediction of the activation fractions of each deformation mode during tension tests along RD (a) and TD (b) based on orientation distributions in Fig. 10.

The changes in mechanical properties of alloys were closely related to deformation mechanisms, and the activation of deformation modes was closely related to CRSS and Schmid factors. For magnesium alloys, plastic deformation temperature was the main factor affecting the CRSS value of the alloy. As tensile tests were conducted at room temperature, temperature was an invariant during the tensile process, and the Schmid factor was related to the direction of tension during the tensile test. Therefore, when conducting mechanical property tests with unchanged tensile direction, crystal orientation was the only variable that affected the deformation mechanism of the alloy. In that way, in order to further analyze the above changes in yield strength of WE43 magnesium alloy during multi-pass hot rolling, an orientation distribution map was used to represent the deformation mode in the alloy structure, as shown in Fig. 10. Meanwhile, Fig. 11 showed the statistical graph of activation scores for different deformation mechanisms of the WE43 magnesium alloy. As reported by Xin, when the CRSS ratio of basal slip, tensile twinning and prismatic slip was set to be 1:1:2, the dominant

deformation modes were tensile twinning with $\theta=0^{\circ}$ - 23° , basal slip with $\theta=23^{\circ}$ - 77° and prismatic slip with $\theta=77^{\circ}$ - 90° (θ was the angle between the stretching direction and the base normal during the stretching experiment)[33]. In this mechanical performance test, the RD and TD of the rolled sheets were selected. In Fig. 11, blue, red, and green respectively represented the main deformation mechanisms of this grain during the stretching process, which were tensile twinning, basal slip, and prismatic slip.

The 23° - 77° grains number of the initial material was obviously higher than the 77° - 90° grains along the ED and only a very small number of 0° - 23° grains were present (Fig. 10a). Whereas along the TD, the initial material had a similar grain number between the 23° - 77° and the 77° - 90° and both were larger than the number of 0° - 23° grains (Fig. 10b). Such distributions were consistent with the activation fractions of deformation mode (Fig. 11). That was to say, the dominant deformation mode was the basal slip along the ED (basal slip: 78.9%, prismatic slip: 20.1%) while were the prismatic and basal slip in the majority with a minor supplement of tension twinning along the TD (basal slip: 51%, prismatic slip: 34.2%, tension twinning: 14.8%).

As the rolling progressed, the 23° - 77° grains decreased to 30.5% from 78.9%, but the 77° - 90° grains increased to 69.3% from 20.1% obviously along the RD. However, along the TD, 0° - 23° grains decreased to 5.1% from 14.8%, while the 23° - 77° grains and 77° - 90° grains increased to 54.6% from 51% and to 40.3% from 34.2%. In general, as rolling proceeded, basal slip significantly decreased but prismatic slip noticeably increased along the RD. Along the TD, tensile twinning decreased, while basal slip and prismatic slip increased.

Different texture produced the activation of different deformation modes, which in turn had an effect on the mechanical properties. Given the similar burgers vectors between the prismatic and basal

slip[33], the deformation mode strengthening was primarily caused by the CRSS whose value was prominently lower for basal slip than prismatic slip. As the basal slip showed the lowest CRSS value, it was the easiest to be activated. However, the basal slip could not satisfy the deformation requirement, thereby the prismatic slip was activated. Due to the higher CRSS of prismatic slip, only when the external stress achieved high enough could it activate the prismatic slip and produce yield behavior, hence presenting higher yield stress, which was consistent with results in the literature[14,34–35]. Therefore, when the grain size was fixed, the activations of prismatic slip produced higher yield stress than the basal slip. For example, the yield stress significantly increased with the decreased activation of basal slip and the increase of activation of prismatic slip along the RD. However, along the TD, due to the slight increase in prismatic and basal slip and the reduction in tensile twinning, the increase in yield strength was weaker than RD.

3.4. Strengthening mechanism

In this work, many factors contributed to the yield stress of the WE43 magnesium alloys after multi-pass hot rolling, such as fine grain strengthening(σ_{gb}), solid solution strengthening(σ_{ss}), dislocation strengthening(σ_d), precipitation strengthening(σ_p). The contribution of each strengthening mechanism to the YS was calculated below.

According to the Hall-Petch relationship, the increment of strength caused by grain refinement could be given by Eq. (1)[36–38]:

$$\sigma_{gb} = \sigma_0 + kd^{-\frac{1}{2}} \quad (1)$$

where σ_0 , k , and d were the lattice friction stress, Hall-Petch slope, and the average grain size, respectively. The σ_0 and k were about 16 MPa and 135 MPa $\mu\text{m}^{0.5}$ [36,39]. Therefore, the fine grain strengthening values for the Initial, Pass 1, Pass 2, Pass 3 sheet were approximately 39.1, 39.9,

51.1, and 61.4 MPa, respectively.

The strength enhanced by the solid solution atom could be written as Eq. (2)[36]:

$$\sigma_{ss} = \sigma_1 + 3.1\varepsilon GC^{\frac{1}{2}}/700 \quad (2)$$

where σ_1 was the yield strength of pure Mg (21 MPa), ε was measured to be 0.74[36], G was the shear modulus (16.6 GPa), and C was the concentration of rare earth solutes. Based on the EDS result of the WE43 alloy (Fig. 2d), the content of rare earth element was approximately 1.55 at.%. Therefore, the strength increment was calculated as 28 MPa.

According to the Bailey-Hirsch equation, the increment of strength influenced by dislocation strengthening could be given by Eq. (3)[36,40]:

$$\sigma_d = \alpha M G b \sqrt{\rho_{GND}} \quad (3)$$

where α was a constant 0.2, M was the Taylor factor, G was the shear modulus (16.6 GPa), b was the Burger vector (0.32 nm), and ρ_{GND} was the dislocation density. The M and ρ_{GND} were calculated by the method in the recently published literature based on our previous work[41]. The calculation results were shown in Table 3. Therefore, the dislocation strengthening values for the Initial, Pass 1, Pass 2, Pass 3 sheet along the RD were calculated as 48.6, 113.0, 117.0, and 127.6 MPa and the corresponding dislocation strengthening values along the TD were approximately 44.7, 88.6, 92.8, and 100.8 MPa, respectively.

Table 3. Calculation results of dislocation density and taylor factor of WE43 magnesium alloys

Sample	$\rho_{GND} / \text{m}^{-2}$	M	
		RD	TD
Initial	1.86×10^{14}	3.35	3.08
Pass 1	7.32×10^{14}	3.91	3.09
Pass 2	7.78×10^{14}	3.95	3.15

The precipitation strengthening based on Orowan mechanism could be written as Eq. (4)[37–38,40]:

$$\sigma_p = M \frac{Gb}{2\pi\sqrt{1-\nu}} \left(\frac{1}{\sqrt{\frac{\pi}{4f-1}}} \right) d_p \ln \frac{d_p}{b} \quad (4)$$

where M was the Taylor factor according to Table 3, G was the shear modulus (16.6 GPa), b was the Burger vector (0.32 nm), ν was the Poisson ratio (0.35), d_p was the average diameter of precipitates, and f was the volume fraction of precipitates, according to the f and d_p in Fig 2 and Fig 4. Therefore, the precipitation strengthening values for the Initial, Pass 1, Pass 2, Pass 3 sheet along the RD were calculated as 33.1, 93.8, 110.7, and 121.0 MPa and the corresponding precipitation strengthening values along the TD were approximately 30.4, 71.6, 87.3, and 95.7 MPa, respectively.

Based on the above, the calculated yield strength values of WE43 alloys after multi-pass hot rolling along the RD and TD were showed in Fig.12. These predicted values were basically consistent with the experimental values with average deviation 5-9%, which correctly predict the increasing trend of YS.

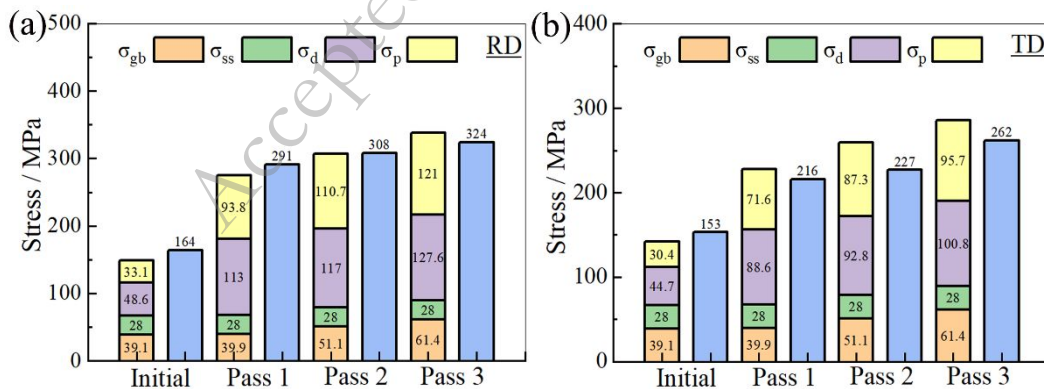


Fig. 12. Respective contribution of the strengthening to WE43 alloys after multi-pass hot rolling: (a) along the RD; (b) along the TD.

In addition, Fig. 13 showed the comparison of YS and EL between the WE43 alloy after multi-pass hot rolling in this study and other rolled or deformed WE43 alloys[13,42–48]. It could be seen that multi-pass hot rolling could effectively improve the YS of WE43 magnesium alloy. At the same time, WE43 magnesium alloy also had excellent plasticity after multi-pass hot rolling.

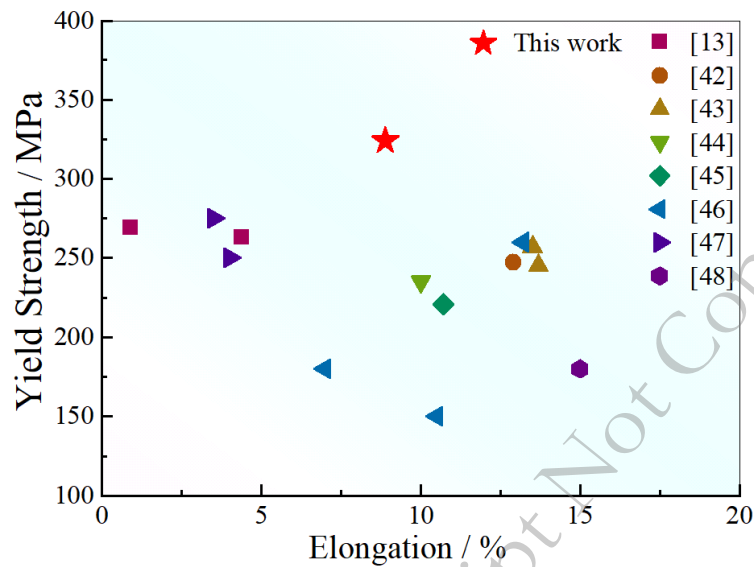


Fig. 13. Comparison of the YS and EL of WE43 alloy after multi-pass hot rolling and other rolled or deformed WE43 alloys in other literatures[13,42–48].

4. Conclusions

(1) Multi-pass hot rolling promoted the formation of small second phases. Such phases were conducive to the dynamic recrystallization and with the help of multiple dynamic recrystallization, the microstructure homogeneity of the resulting sheet was significantly improved and its average grain size was refined to 8.83 μm from 34.3 μm of the initial material.

(2) The rolling deformation rotated abundant grain c-axes toward the ND during the multi-pass hot rolling, enhancing the basal texture strength. The fiber basal texture gradually transferred into the (0002) basal texture owing to the deformation mode activation from basal slip and tension twinning to prismatic slip. Meanwhile, one strengthened $\langle 10\text{-}10 \rangle // \text{RD}$ texture component developed in the (10-10)

pole figure during rolling.

(3) The YS along the RD was significantly improved to 324 MPa in the Pass 3 sheet from 164 MPa in the initial material based on fine-grained strengthening, precipitation strengthening and texture modification. There was an obvious anisotropy between the RD and the TD during the tensile test where the yield strength along the RD was higher about 51MPa than that along the TD (RD: 160 MPa, TD: 109 MPa). The deformation mechanism distribution maps indicated that the RD strong basal texture made its prismatic slip activated more, and therefore produced the higher yield strength owing to the higher critical resolved shear stress of prismatic slip.

Acknowledgments

This work was supported by National Natural Science Foundation of China (Grant No. 52205344, 51925401), Postdoctoral Research Foundation of China (Grant No. 2023M732398), National Key Laboratory Foundation of Science and Technology on Materials under Shock and Impact (Grant No. WDZC2023-1) and Key Research and Development Program of Shandong Province (Grant No. 2023CXPT066).

References

- [1] S.V.S. Prasad, S.B. Prasad, K. Verma, R.K. Mishra, V. Kumar, and S. Singh, The role and significance of Magnesium in modern day research-A review, *J. Magnes. Alloy.*, 10(2022), No. 1, p. 1.
- [2] J. Song, J. She, D. Chen, and F. Pan, Latest research advances on magnesium and magnesium alloys worldwide, *J. Magnes. Alloy.*, 8(2020), No. 1, p. 1.
- [3] M. Liu, Y. Guo, J. Wang, and M. Yergin, Corrosion avoidance in lightweight materials for automotive applications, *NPJ Mater. Degrad.*, 2(2018), No. 1.
- [4] J.L. Wang, J.K. Xu, C. Hopkins, D.H.K. Chow, and L. Qin, Biodegradable Magnesium-Based Implants in Orthopedics—A General Review and Perspectives, *Adv. Sci.*, 7(2020), No. 8.
- [5] J. Xie, J. Zhang, Z. You, S. Liu, K. Guan, R. Wu, J. Wang, and J. Feng, Towards developing Mg alloys with simultaneously improved strength and corrosion resistance via RE alloying, *J. Magnes. Alloy.*, 9(2021), No. 1, p. 41.
- [6] H. Somekawa, A. Kinoshita, K. Washio, and A. Kato, Enhancement of room temperature stretch formability via grain boundary sliding in magnesium alloy, *Materials Science and Engineering: A*, 676(2016), p. 427.

- [7] F. Penghuai, P. Liming, J. Haiyan, C. Jianwei, and Z. Chunquan, Effects of heat treatments on the microstructures and mechanical properties of Mg–3Nd–0.2Zn–0.4Zr (wt.%) alloy, *Materials Science and Engineering: A*, 486(2008), No. 1-2, p. 183.
- [8] A. Barylski, K. Aniolek, G. Dercz, I. Matuła, J. Rak, and I. Mazur, The Effect of Changes in the Aging Temperature Combined with Deep Cryogenic Treatment on the Structure, Phase Composition, and Micromechanical Properties of the WE43 Magnesium Alloy, *Materials*, 16(2023), No. 23, p. 7447.
- [9] M. Daghigh, M. Mohri, H. Ghanbari, and M. Nili-Ahmadabadi, The effect of thermal and strain-induced aging on the mechanical behavior of room temperature ECAP processing of WE43 magnesium alloy, *Journal of Materials Research and Technology*, 24(2023), p. 8508.
- [10] F. Liu, C. Chen, J. Niu, J. Pei, H. Zhang, H. Huang, and G. Yuan, The processing of Mg alloy micro-tubes for biodegradable vascular stents, *Materials Science and Engineering: C*, 48(2015), p. 400.
- [11] N.S. Martynenko, E.A. Lukyanova, V.N. Serebryany, M.V. Gorshenkov, I.V. Shchepinin, G.I. Raab, S.V. Dobatkin, and Y. Estrin, Increasing strength and ductility of magnesium alloy WE43 by equal-channel angular pressing, *Materials Science and Engineering: A*, 712(2018), p. 625.
- [12] S. Amani and G. Faraji, Recrystallization and mechanical properties of WE43 magnesium alloy processed via cyclic expansion extrusion, *International journal of minerals, metallurgy and materials*, 25(2018), No. 6, p. 672.
- [13] B. Liu, L. Xue, R. Li, L. Zong, H. Zhang, J. Li, S. Li, and D. Wu, Plasticity damage behavior caused by compression twins and double twins in rolled WE43 magnesium alloys, *Mater. Lett.*, 350(2023), p. 134877.
- [14] W. Wang, W. Chen, W. Zhang, G. Cui, and E. Wang, Effect of deformation temperature on texture and mechanical properties of ZK60 magnesium alloy sheet rolled by multi-pass lowered-temperature rolling, *Materials Science and Engineering: A*, 712(2018), p. 608.
- [15] A. Dobkowska, A. Zielińska, I. Paulin, Č. Donik, M. Koralnik, B. Adamczyk Cieslak, M. Wiczorek-Czarnocka, D. Kuc, J. Kubasek, T. Mikuszewski, M. Godec, and J. Mizera, Microstructural, corrosion and mechanical properties of a WE43 alloy: conventional extrusion versus SPD, *J. Alloy. Compd.*, 976(2024), p. 173090.
- [16] X. Wang, C. Liu, L. Xu, H. Xiao, and L. Zheng, Microstructure and mechanical properties of the hot-rolled Mg–Y–Nd–Zr alloy, *J. Mater. Res.*, 28(2013), No. 10, p. 1386.
- [17] H. Wang, J. Li, B. Tang, Y. Wang, H. Luo, B. Guan, X. Chen, K. Zheng, and F. Pan, Heterogeneous deformation-induced strengthening of extruded Tip/WE43 composites, *Mater. Charact.*, 207(2024), p. 113526.
- [18] M. Zha, X. Ma, H. Jia, Z. Hua, Z. Fan, Z. Yang, Y. Gao, and H. Wang, Dynamic precipitation and deformation behaviors of a bimodal-grained WE43 alloy with enhanced mechanical properties, *Int. J. Plast.*, 167(2023), p. 103682.
- [19] A. Imandoust, C.D. Barrett, A.L. Oppedal, W.R. Whittington, Y. Paudel, and H. El Kadiri, Nucleation and preferential growth mechanism of recrystallization texture in high purity binary magnesium-rare earth alloys, *Acta Mater.*, 138(2017), p. 27.
- [20] W. Wang, G. Cui, W. Zhang, W. Chen, and E. Wang, Evolution of microstructure, texture and mechanical properties of ZK60 magnesium alloy in a single rolling pass, *Materials Science and Engineering: A*, 724(2018), p. 486.
- [21] C.D. Barrett, A. Imandoust, A.L. Oppedal, K. Inal, M.A. Tschopp, and H. El Kadiri, Effect of grain boundaries on texture formation during dynamic recrystallization of magnesium alloys, *Acta Mater.*, 128(2017), p. 270.

- [22] A. Imandoust, C.D. Barrett, T. Al-Samman, K.A. Inal, and H. El Kadiri, A review on the effect of rare-earth elements on texture evolution during processing of magnesium alloys, *J. Mater. Sci.*, 52(2017), No. 1, p. 1.
- [23] W. Chen, J. Ma, C. Cui, W. Zhang, W. Wang, X. Liu, J. Yang, and G. Cui, Texture role in the mechanical property improvement contributed by grain refinement for Mg-2.6Nd-0.55Zn-0.5Zr alloy subjected to extrusion process, *Materials Science and Engineering: A*, 831(2022), p. 142185.
- [24] W. Wang, W. Chen, W. Zhang, G. Cui, and E. Wang, Weakened anisotropy of mechanical properties in rolled ZK60 magnesium alloy sheets with elevated deformation temperature, *J. Mater. Sci. Technol.*, 34(2018), No. 11, p. 2042.
- [25] L. Zhang, W. Chen, W. Zhang, W. Wang, and E. Wang, Microstructure and mechanical properties of thin ZK61 magnesium alloy sheets by extrusion and multi-pass rolling with lowered temperature, *J. Mater. Process. Technol.*, 237(2016), p. 65.
- [26] W. Wang, L. Ma, S. Chai, W. Zhang, W. Chen, Y. Feng, and G. Cui, Role of one direction strong texture in stretch formability for ZK60 magnesium alloy sheet, *Materials Science and Engineering: A*, 730(2018), p. 162.
- [27] Y.N. Wang and J.C. Huang, Texture analysis in hexagonal materials, *Mater. Chem. Phys.*, 81(2003), No. 1, p. 11.
- [28] W. Zhang, X. Liu, J. Ma, W. Wang, W. Chen, Y. Liu, and J. Yang, Evolution of microstructure and mechanical properties of ZK60 magnesium alloy processed by asymmetric lowered-temperature rolling, *Trans. Nonferrous Met. Soc. China*, 32(2022), No. 9, p. 2877.
- [29] J. Ma, W. Zhang, W. Wang, C. Li, W. Chen, C. Cui, J. Yang, and G. Cui, Effect of pre-solution treatment on the texture and the mechanical properties of hot-extruded Mg-2.6Nd-0.55Zn-0.5Zr alloys, *Materials Science and Engineering: A*, 838(2022), p. 142819.
- [30] M. Knezevic, A. Levinson, R. Harris, R.K. Mishra, R.D. Doherty, and S.R. Kalidindi, Deformation twinning in AZ31: Influence on strain hardening and texture evolution, *Acta Mater.*, 58(2010), No. 19, p. 6230.
- [31] Q. Miao, L. Hu, G. Wang, and E. Wang, Fabrication of excellent mechanical properties AZ31 magnesium alloy sheets by conventional rolling and subsequent annealing, *Materials Science and Engineering: A*, 528(2011), No. 22-23, p. 6694.
- [32] Z. Zhang, J. Zhang, J. Wang, Z. Li, J. Xie, S. Liu, K. Guan, and R. Wu, Toward the development of Mg alloys with simultaneously improved strength and ductility by refining grain size via the deformation process, *International journal of minerals, metallurgy and materials*, 28(2021), No. 1, p. 30.
- [33] B. Guan, Y. Xin, X. Huang, P. Wu, and Q. Liu, Quantitative prediction of texture effect on Hall-Petch slope for magnesium alloys, *Acta Mater.*, 173(2019), p. 142.
- [34] H. Shou, J. Zheng, Y. Zhang, D. Long, J. Rao, and Q. Liu, Quasi-in-situ analysis of dependency of deformation mechanism and work-hardening behavior on texture in Mg-2Zn-0.1Ca alloy, *J. Alloy. Compd.*, 784(2019), p. 1187.
- [35] Y. Wang and H. Choo, Influence of texture on Hall-Petch relationships in an Mg alloy, *Acta Mater.*, 81(2014), p. 83.
- [36] C. Sun, H. Liu, Z. Xu, Y. Wu, K. Yan, J. Ju, J. Jiang, F. Xue, J. Bai, and Y. Xin, Refining 18R-LPSO phase into sub-micron range by pre-kinking design and its prominent strengthening effect on Mg97Y2Zn1 alloy, *J. Mater. Sci. Technol.*, 176(2024), p. 13.
- [37] C. Wang, J. Kang, K. Deng, K. Nie, W. Liang, and W. Li, Microstructure and mechanical

- properties of Mg-4Zn-xGd (x=0, 0.5, 1, 2) alloys, *J. Magnes. Alloy.*, 8(2020), No. 2, p. 441.
- [38] B.N. Du, Z.Y. Hu, L.Y. Sheng, D.K. Xu, Y.X. Qiao, B.J. Wang, J. Wang, Y.F. Zheng, and T.F. Xi, Microstructural characteristics and mechanical properties of the hot extruded Mg-Zn-Y-Nd alloys, *J. Mater. Sci. Technol.*, 60(2021), p. 44.
- [39] A. Rahman, M.M. Husain, and N. Prasad, Microstructural and mechanical properties evaluation of Calcium and zinc-modified WE43-based nanocomposites through stir casting for biodegradable applications, *Ceram. Int.*, 50(2024), No. 17, p. 30284.
- [40] S. Wang, W. Zhang, H. Wang, J. Yang, W. Chen, G. Cui, and G. Wang, Microstructures evolution, texture characteristics and mechanical properties of Mg-2.5Nd-0.5Zn-0.5Zr alloy during the high strain rate hot-rolling, *Materials Science and Engineering: A*, 803(2021), p. 140488.
- [41] X. Wang, W. Chen, Y. Yu, W. Wu, W. Wang, D. Fang, W. Zhang, and J. Sun, Enhancing yield strength and quantifying relationship with microstructure in magnesium alloys through work hardening, *J. Magnes. Alloy.*(2024).
- [42] X. Huang, K. Suzuki, and Y. Chino, Static recrystallization and mechanical properties of Mg-4Y-3RE magnesium alloy sheet processed by differential speed rolling at 823 K, *Materials Science and Engineering: A*, 538(2012), p. 281.
- [43] Q. Li, H. Yan, H. Liu, and R. Chen, Dynamic recrystallization mechanism and near-isotropic mechanical properties of WE43 magnesium alloy sheets rolled at different temperatures, *Mater. Charact.*, 193(2022), p. 112259.
- [44] X. Wang, C. Liu, L. Xu, H. Xiao, and L. Zheng, Microstructure and mechanical properties of the hot-rolled Mg-Y-Nd-Zr alloy, *J. Mater. Res.*, 28(2013), No. 10, p. 1386.
- [45] X. Zhang, G. Yuan, L. Mao, J. Niu, and W. Ding, Biocorrosion properties of as-extruded Mg-Nd-Zn-Zr alloy compared with commercial AZ31 and WE43 alloys, *Mater. Lett.*, 66(2012), No. 1, p. 209.
- [46] N.S. Martynenko, E.A. Lukyanova, V.N. Serebryany, M.V. Gorshenkov, I.V. Shchetinin, G.I. Raab, S.V. Dobatkin, and Y. Estrin, Increasing strength and ductility of magnesium alloy WE43 by equal-channel angular pressing, *Materials Science and Engineering: A*, 712(2018), p. 625.
- [47] J. Kubásek, D. Dvorský, M. avojský, D. Vojtěch, N. Beronská, and M. Fousová, Superior Properties of Mg-4Y-3RE-Zr Alloy Prepared by Powder Metallurgy, *J. Mater. Sci. Technol.*, 33(2017), No. 7, p. 652.
- [48] W. Sun, B. Wu, H. Fu, X. Yang, X. Qiao, M. Zheng, Y. He, J. Lu, and S. Shi, Combining gradient structure and supersaturated solid solution to achieve superior mechanical properties in WE43 magnesium alloy, *J. Mater. Sci. Technol.*, 99(2022), p. 223.